

# BiLSTM-Based Frame Synchronization for Overlapped S-AIS Signals: A Learning-Empowered Approach

Tiancheng Yang<sup>1</sup>, Dongxuan He<sup>1</sup>, Zhiping Lu<sup>2,3</sup>, Hua Wang<sup>1</sup>, Hongye Zhao<sup>1</sup>, Zheng Wu<sup>1</sup>

<sup>1</sup> School of Information and Electronics, Beijing Institute of Technology, Beijing, China

<sup>2</sup> State Key Laboratory of Wireless Mobile Communications, China Academy of Telecommunications Technology, Beijing, China

<sup>3</sup> Beijing University of Posts and Telecommunications, Beijing, China

{3120210823, dongxuan\_he}@bit.edu.cn, luzp@cict.com, {wanghua, 1120191949, 3120220742}@bit.edu.cn

**Abstract**—In this paper, focusing on the signal detection of space-borne automatic identification system (S-AIS), two learning-empowered frame synchronization methods are proposed, which predict the accurate overlapping position of two S-AIS signals with the help of a bidirectional long short-term memory (BiLSTM) network. In particular, by regarding the frame synchronization as a binary classification issue, BiLSTM network can be utilized to find the overlapping position of the received signals accurately. Furthermore, convolutional neural network (CNN) is introduced into the proposed BiLSTM-based approach to handle the non-smooth power fluctuation. Simulation results show that our proposed learning-empowered methods outperform the conventional frame synchronization method in terms of accuracy and robustness, which can work effectively even under various communication conditions.

**Index Terms**—S-AIS communication systems, frame synchronization, BiLSTM, CNN

## I. INTRODUCTION

The automatic identification system (AIS) has been regarded as an essential tool for ship tracking and collision prevention, which can guarantee the safety of vessels and identify friendly and hostile ships. The International Telecommunications Union (ITU) defines two types of AIS structures, namely, terrestrial AIS (T-AIS) and space-borne automatic identification system (S-AIS). In particular, T-AIS is used for ship-to-ship or ship-to-shore communication, while S-AIS is used for ship-to-satellite. S-AIS employs low Earth orbit (LEO) satellites to monitor and track ships in the ocean, especially when ships are out of the coverage of ground monitoring stations. Ships equipped with AIS transponders automatically broadcast both static information (ship name, ship type, etc.) and dynamic information (position, speed, navigation status, etc.) at regular intervals [1]. Traditionally, ships are allocated with carrier frequencies AIS-1 (161.975 MHz) and AIS-2 (162.025 MHz) for communication. In the past decades, two additional frequencies, channel 75 and 76, which are at frequencies 156.775 MHz and 156.825 MHz respectively, have been allocated for long-range AIS service. Long-range AIS provides a higher ship detection probability, even when AIS signals are received by satellites at orbital altitudes up to 1000 km [2].

The use of S-AIS, where the receiver is located on LEO satellites, can greatly expand the coverage of terrestrial AIS.

However, there are several great challenges needed to be addressed [3] - [4]. One major challenge is message collision, which significantly impacts the system performance. In terrestrial AIS, vessels avoid collision with the help of self-organized time-division multiple access (SOTDMA). However, a satellite would cover multiple SOTDMA cells within its field of view (FOV) in S-AIS, which results in colliding between cells in the same time-division multiple access (TDMA) time slot. Additionally, long delays may cause collisions between different time slots. These collisions result in significant interference among multiple users, thus making signal detection and synchronization more difficult [5]. To this end, synchronization should be studied to ensure the reception performance.

Currently, many works have been studied to improve the synchronization performance. For example, a packet detection algorithm was proposed in [5] to perform a coarse frame synchronization, which can distinguish the signal from background noise. Researchers proposed an advanced satellite-based receiver to realize the synchronization and the demodulation of overlapped signals [6] - [7], which utilized a conventional minimum-shift keying (MSK) synchronization scheme [8] - [9] to perform the joint frequency and timing recovery. However, there are few studies about the overlapping position estimation in frame synchronization, especially in the situation that the overlapped signals have similar power levels and Doppler shifts.

Recently, deep learning has shown great potential in solving signal processing problems [10], such as channel estimation [11], automatic modulation classification (AMC) [12], signal demodulation [13], signal prediction [14], etc. In regard to synchronization problem, researchers have paid much attention to improve its accuracy with the help of deep learning. For example, Kalade *et al.* utilized fully convolutional networks (FCNs) for radio physical layer frame synchronization [15]. However, the existing methods cannot effectively address the synchronization problem in complicated communication environments. More specifically, when the noise and interference are severe, the synchronization performance suffers significant degradation.

In this paper, to improve the synchronization performance in the face of overlapped signals in S-AIS system, two learning-empowered frame synchronization methods are proposed. Our

main contributions are summarized as follows:

1) Based on the BiLSTM network, a learning-empowered approach for frame synchronization is proposed. The power fluctuation sequence corresponding to the received overlapped S-AIS signals is used as training samples and classification criteria for the BiLSTM network, which can easily exhibit the features of the overlapped frame header and trailer. By analyzing the characteristics of the power fluctuation sequence, synchronization is transformed into a binary classification task.

2) Based on our proposed BiLSTM-based approach, convolutional neural network (CNN) is introduced into the BiLSTM-based method to improve the synchronization performance further. The one-dimensional CNN network is used to extract features from the power fluctuation sequence, the results of which is then input into the BiLSTM network. Such approach has good robustness, which achieves superior results in complex communication environments with high noise and interference.

This paper is organized as follows. Section II introduces the AIS system and its practical challenges. Section III details our proposed BiLSTM-based synchronization method. Section IV presents the simulation results and analysis. Finally, Section V concludes the whole paper.

## II. SYSTEM MODEL

### A. Frame Format

To ensure transmission efficiency and reliability, S-AIS frame typically includes a preamble, a message, and error checking codes. The user's payload is utilized to perform a cyclic redundancy check (CRC), which adds a 16-bit frame check sequence to the end of the 96-bit payload, thus resulting in a 112-bit data sequence with CRC verification codes. The bit-flipping operation is applied to the 112-bit data sequence, where the first and last 16 bits are flipped by changing '0' to '1' and '1' to '0'. Next, the 112-bit data sequence is searched for five consecutive '1' from the start to the end, and one '0' is inserted behind each of them. This step ensures that the data sequence does not have six consecutive '1', thus avoiding confusion of the frame header and trailer positions during transmission. Next, an 8-bit sequence  $[0, 1, 1, 1, 1, 1, 1, 1, 0]_b$  is inserted to the start and the end of the 112-bit data sequence, which attaches the frame header and trailer. The processed sequence should be concatenated with a '01' or '10' repeated bit synchronization sequence whose length is 24, before it, an 8-bit signal rising edge should be reserved to guarantee signal stability. After adding 32-bit information, a buffered sequence is connected to the frame trailer, thus resulting in a whole frame size of 256 bits.

Subsequently, non return zero inverted (NRZI) coding scheme is employed to the entire frame to obtain the completed data packet whose time occupation is 26.67 milliseconds, i.e., a slot and a superframe of S-AIS consists of 2250 completed data packets, which occupies 1 minute in time domain, as shown in Fig. 1.

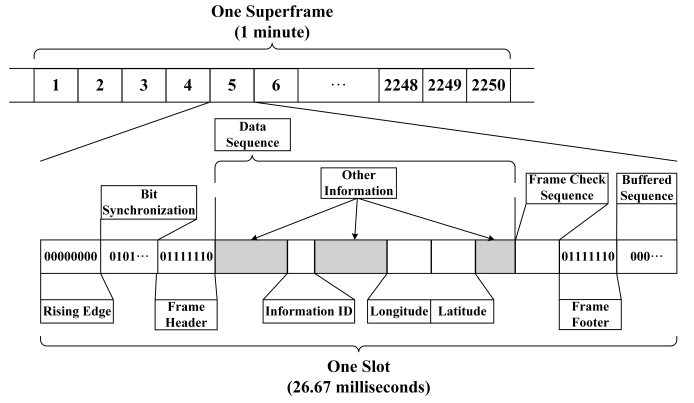


Fig. 1. The format of the S-AIS signal.

### B. Signal Generation

Gaussian minimum shift keying (GMSK) is adopted in S-AIS, which is realized by adding a Gaussian pre-modulation filter before a typical MSK modulator. Gaussian filtering process leads to smoother phase path, which can effectively reduce the spectral width and sidelobe. Therefore, GMSK has a compact power spectral density and high spectral efficiency. Additionally, GMSK modulation has strong anti-interference capabilities due to its constant envelope and narrow bandwidth characteristics, thus making it a popular choice for wireless communication systems in noisy environments.

The generation of S-AIS signals is shown in Fig. 2. The 256-bit frame sequence is represented by  $x(t)$ , which has undergone the NRZI transform, and  $g(t)$  can be acquired by applying a Gaussian filter to  $x(t)$ , whose impulse response can be expressed as  $g_s(t)$ , i.e.,  $g(t) = x(t) * g_s(t)$ , where  $g_s(t)$  is given by

$$g_s(t) = \frac{1}{\sqrt{2\pi}\sigma} e^{-\left(\frac{t^2}{2\sigma^2}\right)}, \quad (1)$$

where  $\sigma = \frac{1}{2\pi B}$  denotes the bandwidth-time product of the Gaussian filter, and  $B$  is the 3 dB bandwidth of the filter.

Additionally,  $g_{int}(t)$  is obtained by integrating  $g(t)$  from 0 to  $T$  first, where  $T$  is the bit duration. Hilbert transform, denoted as  $\mathcal{H}$ , should be applied to  $\Re\{s(t)\}$  to obtain the final S-AIS complex signal  $s(t)$ , where  $\Re\{\cdot\}$  is the real part. The Hilbert transform is given by

$$s(t) = \mathcal{H}[\Re\{s(t)\}] = \frac{1}{\pi} \lim_{\epsilon \rightarrow 0} \left( \int_{-T}^{t-\epsilon} \frac{\Re\{s(\tau)\}}{t-\tau} d\tau + \int_{t+\epsilon}^T \frac{\Re\{s(\tau)\}}{t+\tau} d\tau \right), \quad (2)$$

where  $\epsilon$  is a positive number that tends towards 0.

### C. Problem Formulation

Due to the mutual contamination among overlapped S-AIS signals, the overlap of multiple S-AIS signals is an intractable problem for practical applications, which could lead to a severe performance degradation. More specifically, as illustrated in Fig. 3, the FOV of the satellite is so broad that the satellite can cover hundreds of SOTDMA areas simultaneously, which

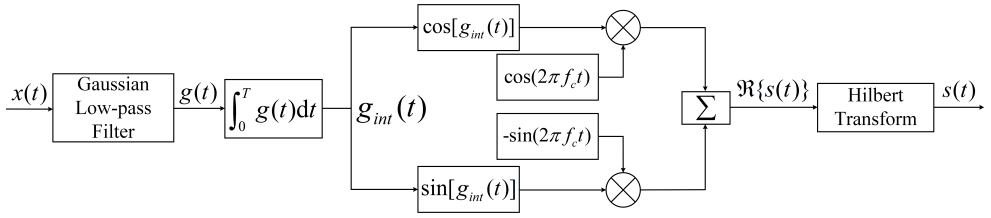


Fig. 2. The generation of S-AIS signal in engineering applications.

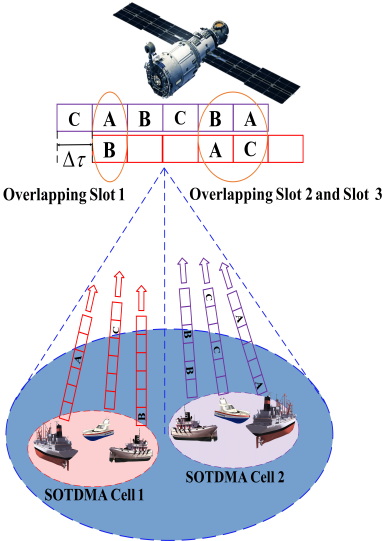


Fig. 3. The system model of S-AIS.

makes the overlapped signals to be influenced by signals from different cells.

In this work, we concentrate on two SOTDMA cells within the satellite's FOV. It is worth noting that the time delay, denoted by  $\Delta\tau$ , is caused by the inconsistent distance from different cells to a specific sub-satellite point. In practice, the superposition of two S-AIS signals is typically considered since it is almost impossible to demodulate all S-AIS signals when more than two S-AIS signals are received simultaneously. In such cases, only the signal with the highest power is most likely to be demodulated, while the demodulation of other signals depends on the degree of reconstruction. Therefore, our research focuses on two overlapped S-AIS signals with independent Doppler shifts, time delays, phase offsets, and signal-to-noise ratios (SNRs), which can be mathematically expressed as

$$y(t) = \underbrace{A_1 s_1(t) e^{j(2\pi\Delta f_1 t + \theta_1)}}_{x_1} + \underbrace{A_2 s_2(t - \Delta\tau) e^{j(2\pi\Delta f_2(t - \Delta\tau) + \theta_2)}}_{x_2} + w(t). \quad (3)$$

More specifically,  $x_1$  represents the first S-AIS signal with amplitude  $A_1$ , baseband signal  $s_1(t)$ , Doppler shift  $\Delta f_1$ , and phase offset  $\theta_1$ ,  $x_2$  represents the second S-AIS signal with amplitude  $A_2$ , baseband signal  $s_2(t - \Delta\tau)$ , Doppler shift  $\Delta f_2$ , and phase offset  $\theta_2$ .  $w(t)$  represents the additive Gaussian white noise.

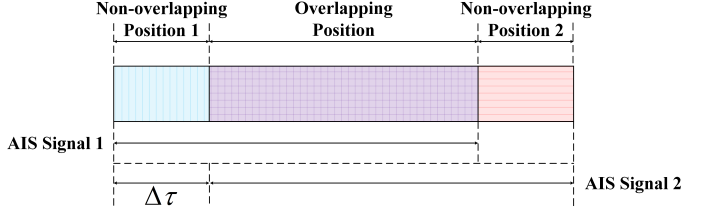


Fig. 4. The illustration of overlapped S-AIS signals.

Based on the power difference between two signals, the demodulation methods can be categorized into two main categories, namely, successive interference cancellation (SIC) for signals with significant power difference and blind source separation (BSS) (or sparsity-based reconstruction) for signals with negligible power difference. In order to guarantee the demodulation performance, accurate synchronization methods should be employed to estimate the overlapped header and trailer positions illustrated in Fig. 4. Even if the estimation of overlapped frame header and trailer positions is not very accurate, the performance of signals with obvious power difference would not be greatly affected. However, the accurate overlapped positions need to be obtained for BSS and sparsity-based reconstruction methods for signals with negligible power difference.

### III. PROPOSED FRAME SYNCHRONIZATION METHODS

The conventional methods rely on empirical parameters, resulting in effectiveness and performance degradation under varying environment. To address this problem, two frame synchronization methods are proposed with the help of deep learning.

1) *BiLSTM-based Method*: The BiLSTM network is a bidirectional recurrent neural network consisting of two long short-term memory (LSTM) networks with opposite directions, which is effective in handling time series data. Moreover, the BiLSTM network is able to learn relevant information from both the past and future sequences in sequence data processing. In this work, a novel frame synchronization method based on BiLSTM network is proposed, which transforms the frame synchronization problem into a binary classification task.

The fundamental structure of BiLSTM is illustrated in Fig. 5, which consists of two LSTM chains, namely, the forward and backward LSTM layers. In Fig. 5,  $X_t$  represents the input current state, while  $C_t^i$  and  $h_t^i$  represent the two input past states or current states, and  $h_t$  represents the current state

obtained by the forward and backward LSTM networks, where  $t$  represents a certain time and  $i \in \{f, b\}$  denotes the forward or backward LSTM layers. The rectangular boxes represent the neural network layers to be trained. The circular shapes denote pointwise operations, and two types of activation functions are utilized, namely, *sig* and *tanh*. The *sig* activation function is defined as  $\text{sig}(x) = \frac{1}{1+e^{-x}}$ , while the *tanh* activation function is expressed as  $\text{tanh}(x) = \frac{e^x - e^{-x}}{e^x + e^{-x}}$ . The inputs  $h_{t-1}^f$  and  $X_t$  are first processed by the activation function layer *sig* to obtain  $F_t^f$  as

$$F_t^f = \text{sig}(W_F^f \cdot [h_{t-1}^f, X_t] + b_F^f), \quad (4)$$

where  $W_F^f$  and  $b_F^f$  respectively represent the weights and biases. Next,  $h_{t-1}^f$  and  $X_t$  can be processed by the same method to obtain  $I_t^f$  and  $O_t^f$ , which are calculated as

$$I_t^f = \text{sig}(W_I^f \cdot [h_{t-1}^f, X_t] + b_I^f), \quad (5)$$

$$O_t^f = \text{sig}(W_O^f \cdot [h_{t-1}^f, X_t] + b_O^f), \quad (6)$$

where  $W_I^f$  and  $W_O^f$  represent the weights, while  $b_I^f$  and  $b_O^f$  represent the biases. The parameter  $\tilde{C}_t^f$  can be obtained as

$$\tilde{C}_t^f = \text{tanh}(W_C^f \cdot [h_{t-1}^f, X_t] + b_C^f), \quad (7)$$

where  $W_C^f$  and  $b_C^f$  respectively represent the weights and biases. Finally, the final outputs  $C_t^f$  and  $h_t^f$  can be obtained as

$$C_t^f = F_t^f * C_{t-1}^f + I_t^f * \tilde{C}_t^f, \quad (8)$$

$$h_t^f = O_t^f * \tanh(C_t^f). \quad (9)$$

In terms of training set, the original overlapped signals at the frame header and trailer cannot be easily distinguished, which makes it impossible to train and classify them due to mutual interference. To address this issue, we propose a power fluctuation sequence  $y_{pf}(t)$  of signal  $y(t)$ , which can be calculated as

$$y_{pf}(nT) = \frac{1}{L_{tot}} \sum_{i=n}^{n+L_{tot}-1} |y(iT)|^2, n = 1, 2, \dots, L_{seq} - L_{tot} + 1 \quad (10)$$

where  $L_{tot}$  represents the number of total samples used in each power fluctuation computation, and  $L_{seq}$  is the length of this received S-AIS overlapped signal  $y(t)$ . Compared to  $y(t)$ ,  $y_{pf}(t)$  has more distinct features and is more robust to inter-user interference. In Fig. 6, two sliding windows with a length of  $L_w$  slide from the start and the end of the power fluctuation sequence  $y_{pf}(t)$ , and the items within two windows are fed into the trained BiLSTM network at each step. For the binary classification problem derived from the synchronization problem, when the overlapped frame header or trailer is located in the center of the sliding window, the final classification result is set to be 1, and the classification results

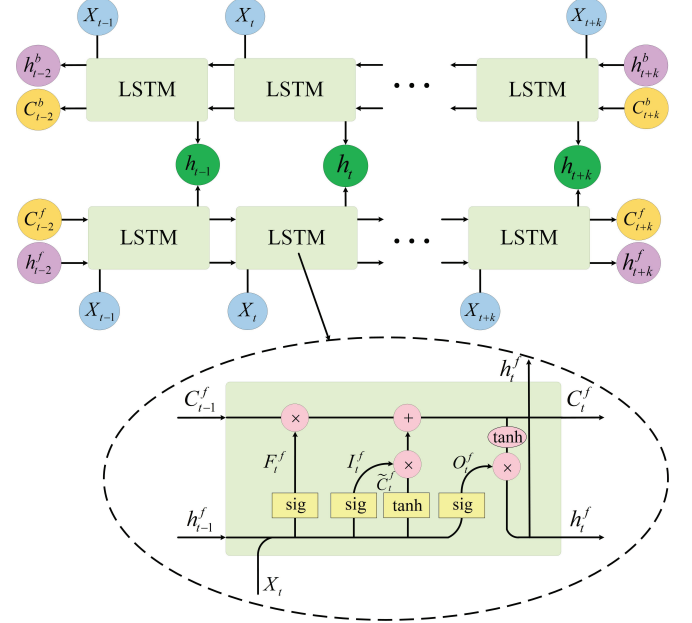


Fig. 5. The fundamental principle model of BiLSTM.

for other cases are 0. Thus, the position of the overlapped frame header or trailer is determined as the point with the maximum probability among those classified as 1.

For the gradient descent algorithm, adaptive moment estimation (Adam) is selected [16], which can dynamically adjust the learning rate at different time steps to improve the training efficiency and stability. For Adam, the initial learning rate is set to  $10^{-3}$ , the maximum training epochs is set to 200, the gradient threshold is set to 2, the batch size used for each training step is set to 20, and the loss function is cross-entropy.

2) *CNN-BiLSTM-based Method*: CNN can automatically extract features and perform classification, which has good robustness and interpretability. Therefore, a modified frame synchronization method based on CNN-BiLSTM is proposed to handle the non-smoothness that is hard to be solved by conventional filtering methods. Based on the BiLSTM network, a one-dimensional CNN network is employed to extract features from the data within two sliding windows before inputting them into the BiLSTM network, as illustrated in Fig. 6. This approach helps to decrease signal interference among users and produce smoother input sequences. Accordingly, the signals can be effectively processed by BiLSTM.

#### IV. SIMULATION RESULTS AND DISCUSSION

In this section, simulation results are presented to verify the effectiveness of our proposed BiLSTM-based synchronization methods. Throughout this section, two S-AIS signals with random frequency offset, phase offset, and time delay are considered. The energy per bit to noise power spectral density ratio ( $E_b/N_0$ ) is set from 20 dB to 25 dB, which is commonly observed among most ships within the satellite's FOV [2]. The signal-to-interference ratio (SIR) between the two signals is selected as 0 dB and 2 dB to simulate the scenario of

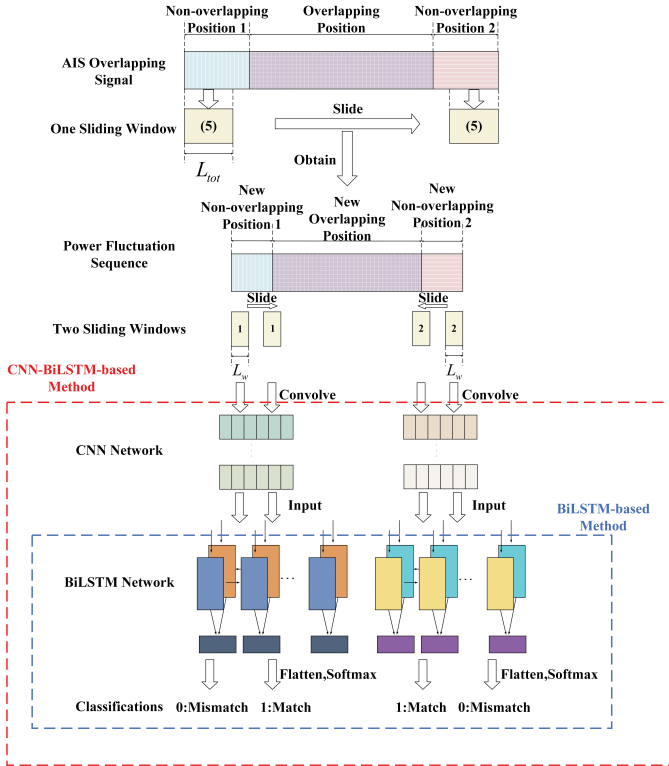


Fig. 6. The principle of the learning-empowered methods.

high mutual interference. Moreover, when there is a power difference between the two signals, the one with higher power arrives first, making it more challenging to synchronize the overlapped frame header and trailer positions of the signal with lower power.

It should be noted that certain precise communication synchronization techniques, such as the autocorrelation scheme, cannot be applied in the S-AIS communication environment due to its susceptibility to interference from other signals. For comparison, the double sliding window method is considered, which is based on sliding window in both time and frequency domains to realize synchronization [17].

For the BiLSTM-based method, three forward and backward LSTM layers are adopted, the number of neurons in each layer is 20. For the CNN network, five 6x1 convolutional kernels are selected to smooth the power fluctuation sequence. The lengths of the downsampled power fluctuation sequence input into the two learning-empowered schemes each time are both 60x1.

Fig. 7 illustrates the detection probability of overlapped frame headers when the timing error is within one symbol period. It can be observed that, the performance of the double sliding window method increases with the increase of  $E_b/N_0$ , however, the detection performance suffers significant degradation. The conventional double sliding window algorithm synchronizes the received S-AIS signal by directly using the power feature to search for the overlapped frame header and trailer. However, the frame header, trailer, and the bit

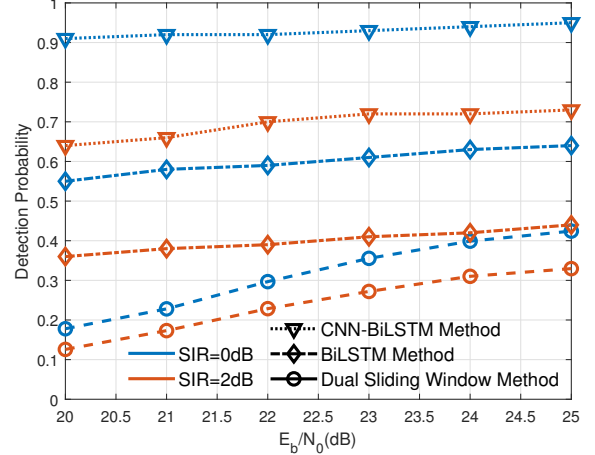


Fig. 7. The overlapped frame header detection probability (timing error within one symbol period) comparison of different frame synchronization schemes and different SIR with different  $E_b/N_0$ .

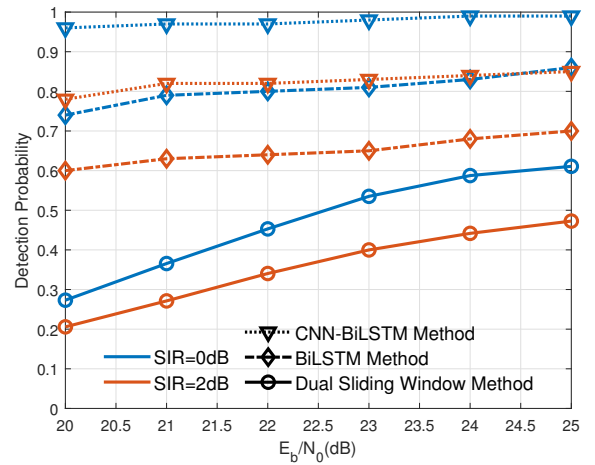


Fig. 8. The overlapped frame header detection probability (timing error within two symbol periods) comparison of different frame synchronization schemes and different SIR with different  $E_b/N_0$ .

synchronization sequence fail to follow strict orthogonality, thus leading to insignificant power features of the overlapped frame header and trailer. In contrast, our proposed learning-empowered schemes exhibit excellent robustness and achieve superior detection performance when compared to the double sliding window method. For example, the detection probability of the two schemes remains almost unchanged in the range of  $E_b/N_0$  from 20 dB to 25 dB. Moreover, when the  $E_b/N_0$  is 25 dB and SIR is 0 dB and 2 dB, the detection probability of double sliding window method is about 0.4 and 0.3, while the detection probability of the BiLSTM-based method is about 0.65 and 0.45, respectively, and the detection probability of the CNN-BiLSTM-based method is about 0.95 and 0.75, respectively, which shows the effectiveness of our proposed learning-empowered methods.

In Fig. 8, we present the detection probability of overlapped frame headers when the timing error is within two symbol periods. We can see that, the performance of the double sliding window method increases with the increase of  $E_b/N_0$ , and the detection probability can reach about 0.6 and 0.5 when SIR is 0 dB and 2 dB in the condition of  $E_b/N_0$  being 25 dB, respectively. In contrast, our proposed learning-empowered schemes still show excellent robustness and performance, detection probability of which is above 0.6 under varying communication conditions, which is due to the fact that our proposed BiLSTM-based method directly utilizes the power fluctuation features of the overlapped frame header and trailer. As BiLSTM considers both the past and future features of the power fluctuation sequence, the features of the overlapped frame header and trailer are more significant, thus resulting in better synchronization performance than the double sliding window algorithm. In addition, the one-dimensional CNN network in the CNN-BiLSTM-based method first extracts features from the power fluctuation sequence and then inputs the extracted sequence to the BiLSTM network, which results in better performance.

## V. CONCLUSIONS

In this paper, we proposed two novel learning-empowered frame synchronization methods for S-AIS communication systems to achieve accurate frame synchronization when the signals are overlapped. Based on a BiLSTM network, our proposed method directly utilizes the power fluctuation features of the overlapped frame header and trailer. However, due to the design flaw of the S-AIS signal frame structure, the power fluctuation features may not always be significant enough for accurate synchronization. To address this issue, we proposed to incorporate a one-dimensional CNN network to extract more features from the power fluctuation sequence before feeding it into the BiLSTM network. This approach significantly improve the accuracy of the overlapping position prediction, which ensures reliable frame synchronization in complicated communication scenarios. Simulation results demonstrated that our proposed learning-empowered methods could achieve good accuracy and robustness compared to conventional methods.

## VI. ACKNOWLEDGMENT

This work was supported in part by the National Key Research and Development Program of China under Grant 2020YFB1807900, in part by State Key Laboratory of Wireless Mobile Communications, China Academy of Telecommunications Technology (CATT), in part by the National Natural Science Foundation of China under Grant 62101306, and in part by Datang Linktester Technology Co. Ltd.

## REFERENCES

- [1] G. Sahay, S. Naskar, H. K. Reddy N and V. D, "A novel architecture and design of FPGA based space-borne AIS receiver," in *Proc. IEEE Int. Conf. Electron., Comput. Commun. Technol. (CONECCT)*, Jul. 2021, pp. 1-6.
- [2] I.-R. M.1371-5, "Technical characteristics for an automatic identification system using time division multiple access in the VHF maritime mobile frequency band," International Telecommunication Union, Recommendation, Feb. 2014.
- [3] J. Carson-Jackson, "Satellite ais developing technology or existing capability," *J. Navig.*, 65, pp. 303-321, 2012.
- [4] M. A. Cervera and A. Ginesi, "On the performance analysis of a satellite-based AIS system," in *Proc. 10th Int. Workshop Signal Process. Space Commun.*, pp. 1-8, 2008.
- [5] W. Lan et al., "A pipelined synchronization approach for satellite-based automatic identification system," in *Proc. IEEE Int. Conf. Commun. (ICC)*, Lumpur, Malaysia, May 2016, pp. 1-6.
- [6] P. Burzigotti, A. Ginesi, and G. Colavolpe, "Advanced receiver design for satellite-based automatic identification system signal detection," *Int. J. Satell. Commun. Netw.*, vol. 30, pp. 52-63, Mar. 2012.
- [7] G. Colavolpe, T. Foggi, A. Ugolini, et al, "A highly efficient receiver for satellite-based automatic identification system signal detection," *J. Satell. Commun. Netw.*, vol. 34, pp. 57-73, Oct. 2014.
- [8] Morelli M and Mengali U, "Joint frequency and timing recovery for MSK-type modulation," *IEEE Trans. Commun.*, vol. 47, no. 6, pp. 938-946, Jun. 1999.
- [9] Morelli M and Mengali U, "Feedforward carrier frequency estimation with msk-type signals," *IEEE Commun. Lett.*, vol. 2, no. 8, pp. 235-237, Aug. 1998.
- [10] T. O'Shea and J. Hoydis, "An introduction to deep learning for the physical layer," *IEEE Trans. Cogn. Commun. Netw.*, vol. 3, no. 4, pp. 563-575, Dec. 2017.
- [11] H. Ye, G. Y. Li and B. -H. Juang, "Power of deep learning for channel estimation and signal detection in OFDM systems," *IEEE Wireless Commun. Lett.*, vol. 7, no. 1, pp. 114-117, Feb. 2018.
- [12] Y. Wang, M. Liu, J. Yang and G. Gui, "Data-driven deep learning for automatic modulation recognition in cognitive radios," *IEEE Trans. Veh. Technol.*, vol. 68, no. 4, pp. 4074-4077, Apr. 2019.
- [13] D. He, Z. Wang, T. Q. S. Quek, S. Chen and L. Hanzo, "Deep learning-assisted TeraHertz QPSK detection relying on single-bit quantization," *IEEE Trans. Commun.*, vol. 69, no. 12, pp. 8175-8187, Dec. 2021.
- [14] J. Chen, W. Li, S. Li, H. Chen, X. Zhao, J. Peng, Y. Chen and H. Deng, "Two-Stage Solar Flare Forecasting Based on Convolutional Neural Networks," *Space Sci Technol.*, 2022.
- [15] S. Kalade, L. H. Crockett and R. W. Stewart, "Training deep filters for physical-layer frame synchronization," *IEEE Open J. Commun. Soc.*, vol. 3, pp. 1063-1075, 2022.
- [16] D. P. Kingma and J. L. Ba, "Adam: A method for stochastic optimization," in *Proc. Int. Conf. Learn. Representations (ICLR)*, 2015.
- [17] Heiskala, J. and Terry, J., *OFDM Wireless LANs: A Theoretical and Practical Guide*. Sams Publishing, 2001.